ADVANCING EARTH AND SPACE SCIENCES

JGR Biogeosciences

RESEARCH ARTICLE

10.1029/2025JG009284

The Timing of Albedo Declines With Reforestation

Christopher A. Williams[1], **Surendra Shrestha**[1], **Susan Cook-Patton**[2], **Natalia Hasler**[1], **Drew E. Terasaki Hart**[2,3], **and Samantha Yeo**[2]

[1]Graduate School of Geography, Clark University, Worcester, MA, USA, [2]The Nature Conservancy, Arlington, VA, USA, [3]CSIRO Environment, Brisbane, QLD, Australia

Key Points:

- Half of the climate warming effect from decreased albedo with reforestation occurs within 40 years, but it takes 50–120 years for 80%
- The slowest declines occur in extra-tropical regions and broadleaf forests and woody savannas
- The fastest declines occur in tropical environments, and for needleleaf or mixed broadleaf-needleleaf forests

Supporting Information:

Supporting Information may be found in the online version of this article.

Correspondence to:

C. A. Williams,
cwilliams@clarku.edu

Citation:

Williams, C. A., Shrestha, S., Cook-Patton, S., Hasler, N., Terasaki Hart, D. E., & Yeo, S. (2026). The timing of albedo declines with reforestation. *Journal of Geophysical Research: Biogeosciences*, *131*, e2025JG009284. https://doi.org/10.1029/2025JG009284

Received 25 JUL 2025
Accepted 31 AUG 2026

Author Contributions:

Conceptualization: Christopher A. Williams
Formal analysis: Christopher A. Williams, Surendra Shrestha, Natalia Hasler
Funding acquisition: Christopher A. Williams
Investigation: Christopher A. Williams
Methodology: Christopher A. Williams, Surendra Shrestha, Susan Cook-Patton, Natalia Hasler, Drew E. Terasaki Hart, Samantha Yeo
Project administration: Christopher A. Williams
Resources: Christopher A. Williams
Supervision: Christopher A. Williams

Abstract Reforestation is a leading climate solution for removing carbon dioxide from the atmosphere, but generally decreases surface albedo, which diminishes its climate mitigation value. Knowing how quickly this albedo effect unfolds relative to carbon removal is critical for planning climate mitigation actions, yet the temporal changes in albedo are poorly described. This study uses satellite observations to characterize temporal changes in albedo with stand development for different forest types and ecoclimatic settings around the world. We find that about half of the climate warming effect from decreased albedo occurs within 40 years, but that it takes anywhere from 50 to 120 years to reach 80% of the full effect. The slowest declines occur in extra-tropical regions and broadleaf forests and woody savannas. The fastest declines occur in tropical environments, and for needleleaf or mixed broadleaf-needleleaf forests. Results were recast as a global map to help inform reforestation practitioners about the time it takes for reforestation's albedo-driven warming to approach its maximum effect.

Plain Language Summary Reforestation is a leading solution for removing carbon dioxide from the atmosphere but also often absorbs more energy from the sun than non-forests (“albedo effect”), causing warming that offsets the cooling benefits of carbon removal. Knowing how quickly this albedo effect unfolds is critical for understanding how the climate benefit of reforestation changes over time. Yet, the temporal changes are poorly described. This study provides a globally comprehensive map of how albedo changes through time for different forest types and ecoclimatic settings. About half of the warming from albedo change occurs within 40 years, but that it takes anywhere from 50 to 120 years to reach 80% of the full effect. The fastest declines are found in tropical, humid environments, and in forests with needleleaf trees. The largest declines appear in temperate environments and in needleleaf or mixed forest types, including cold temperate and boreal regions with substantial wintertime snow cover. These data can help account for the climate benefits of forest change through time.

1. Introduction

As forests grow and develop, they remove atmospheric carbon but reflect less sunlight to space (Betts et al., 2007; Bonan, 2008; Foley et al., 2005; Jackson et al., 2008; Pongratz et al., 2010). The balance of these opposing climate effects varies geographically, with some forested areas leading to net climate cooling and others causing warming (Bathiany et al., 2010; Betts, 2000; Bright et al., 2015; Ghimire et al., 2014; Hasler et al., 2024; Jiao et al., 2017; Lawrence et al., 2022; Pongratz et al., 2010; Williams et al., 2021). What has received less attention is how these effects vary over time as tree cover gradually increases and forests continue to age. This study seeks to fill that gap by documenting temporal variations in albedo with forest stand age, which is needed to characterize the time-dependency of albedo-driven climate forcing with reforestation.

Reforestation, here meaning forest cover expansion in areas where forests would naturally exist as the dominant vegetation type, involves re-establishment of tree cover with progressive growth and development of forest structure and composition through time. Darker, denser forests have lower albedo and absorb more solar radiation compared to other vegetation types such as grasslands (e.g., Gao et al., 2014; Juang et al., 2007; Kirschbaum et al., 2011; Rotenberg & Yakir, 2010; Zhang et al., 2020). Thus, as reforestation progresses, the decline in albedo can be expected to unfold gradually over several decades as forests approach their maximum vegetation cover, experience canopy closure, and develop vertically deep and structurally complex multi-layered and multi-species canopies. Few prior studies have examined such changes, and all report locally specific examples (Amiro et al., 2006; Bright et al., 2018; Drever et al., 2021; Halim et al., 2019; Kuusinen et al., 2014). How these patterns vary over time in different ecoclimatic settings worldwide has yet to be documented.

10.1029/2025JG009284

Visualization: Christopher A. Williams, Surendra Shrestha, Natalia Hasler
Writing – original draft: Christopher A. Williams
Writing – review & editing: Christopher A. Williams, Surendra Shrestha, Susan Cook-Patton, Natalia Hasler, Drew E. Terasaki Hart, Samantha Yeo

Corporations, governments, and individuals are using reforestation projects to meet climate mitigation goals, but an accurate accounting of the climate benefit requires not only adjusting carbon-only estimates for the magnitude of albedo change but also the timing of that change. We have a growing understanding of how forest carbon stocks change through time (e.g., Busch et al., 2024), but we lack a similar understanding for albedo. If albedo changes rapidly, it is possible that reforestation efforts may lead to warming initially even in places where cooling from carbon removal will ultimately outweigh albedo-driven warming. Thus, deployment of reforestation to meet time-bound climate goals requires an improved understanding of how albedo changes through time. Similarly, if carbon credits are to be albedo-adjusted (Riley et al., 2025), we need information on how large albedo adjustments need to be and when they should occur.

Earth observing systems provide widespread measurements of albedo (e.g., Schaaf et al., 2002) that can be readily used to sample albedo dynamics with changes in forest cover (Bright et al., 2015, 2018; Ghimire et al., 2014; Jiao et al., 2017; Rohatyn et al., 2022). Several studies have used these data to characterize changes in albedo with forest development (e.g., Bright et al., 2013, 2018; Halim et al., 2019; Healey et al., 2025; Kuusinen et al., 2014; O'Halloran et al., 2012; Shrestha et al., 2022, 2024; Vanderhoof et al., 2013, 2014), but such studies are often regionalized and few, if any, global analyses exist.

Here, we analyze changes in albedo over time during the process of reforestation by using data sets on land cover, surface albedo, and forest age. We employ a space-for-time substitution approach, creating a chronosequence that tracks the progression from treeless and sparsely treed landscapes—such as grasslands, shrublands, and savannas—to fully mature forests that are up to 150 years old. Our analysis focuses on the timing of albedo changes rather than the magnitude. We address the following questions: How long does it take for albedo to decline to its minimum value with reforestation? What is the shape of decline? How variable is the pace of decline? Is variation in albedo decline related to forest type or ecoclimatic setting? The study's analyses document how albedo varies over time with forest development, examining variations across ecoclimatic settings and forest types around the globe. With albedo change being the dominant biogeophysical effect of land cover change in many parts of the world (Davin & de Noblet-Ducoudre, 2010; Lawrence et al., 2022; Weber et al., 2024), understanding the time-dependency of this important factor is needed to assess the true global climate effects of reforestation.

2. Methods

2.1. Data Sources

2.1.1. Ecoregion Map

To account for spatial variation in albedo change, we quantified changes separately for 74 sampling units (Figure S1 in Supporting Information S1). These sample units were based on ecoregions of Dinerstein et al. (2017) but with aggregation of adjacent smaller ecoregions that share the same biome class and climate type (Beck et al., 2018) to avoid insufficient sample sizes. Ecoregions were distributed over major ecoclimatic zones of the world, with three in boreal forest, seven in Mediterranean forest, four in montane grassland, 10 in temperate broadleaf and mixed forest, seven in temperate coniferous forest, 13 in temperate grassland and savanna, six in tropical deciduous broadleaf forest, five in tropical grassland and savanna, 14 in tropical moist evergreen broadleaf forest, and five in tundra (Figure S1 in Supporting Information S1). We include results for grassland ecosystems for completeness, not to promote afforestation of native grasslands to avoid perverse biodiversity outcomes (Veldman et al., 2015).

2.1.2. Forest Age

To understand how albedo changed through time, we needed to create an albedo chronosequence. To do so, we assigned a forest age to each MODIS pixel using the forest age data developed by Besnard et al. (2021) to assign a forest age to each MODIS pixel. This data product provides a gridded global distribution of forest age estimated with a machine learning approach trained on more than 40,000 forest inventory plots along with additional biomass and climate data. The statistical model used to create this product had an accuracy deemed suitable for this study, with precisions of 0.81 and 0.99 for classifying old-growth and non-old-growth forests, and with a Nash-Sutcliffe efficiency of 0.6 for estimating plot-level forest age, where old-growth forests were defined as stands with an age greater than or equal to 300 years (Besnard et al., 2021). The errors in the forest age data set are sizable, with an RMSE of 48 years and a normalized RMSE of 52%. However, errors appear to be normally distributed (Figure 3b of Besnard et al. (2021) cross-validated results). This would suggest errors impose sizable random noise, but that they will be balanced, meaning they are offsetting in their effects on our spatial sampling of a median response of albedo to forest age. The forest age data set has some spatial biases (Besnard et al., 2021, Figure 3e), but it is unclear whether this is likely to have influenced this study's main findings. One tendency is underestimation (about +20 years) in western North America despite a high density of forest plots used in model training. Another tendency is overestimation (−20 to −60 years) for forests in western coastal Europe, where few plot data were used in model training. Few other generalizable patterns of bias can be discerned, with many of the largest biases being adjacent to areas with similarly large bias of opposite sign. That would be expected to introduce noise but not bias in the findings presented in this study.

2.1.3. MODIS Land Cover, Albedo, and Snow Cover

To estimate how albedo changes with forest aging, we selected a starting land cover type assumed to be grassland and studied conversion to six possible end forest types - evergreen needleleaf forest (ENF), evergreen broadleaf forest (EBF), deciduous needleleaf forest (DNF), deciduous broadleaf forest (DBF), mixed forest (MF), and woody savanna (WSA). We used several spatially and temporally consistent MODIS products to assess the albedo dynamics of reforestation. We obtained MODIS satellite data for the years 2014–2018 from the MODIS data archive (https://www.earthdata.nasa.gov/). The MODIS products used in this study are provided with a sinusoidal projection and each geographic data tile covers an area of approximately 1,200 km × 1,200 km.

We used the Terra and Aqua combined MODIS version 6 land cover type (MCD12Q1) data product to characterize land cover, providing global land cover types at yearly intervals and 500 m resolution for 2001 to present (Friedl et al., 2002). The MODIS land cover data are prepared using an ensemble decision tree algorithm to a composite of time series acquired within each year for annual mapping. The input time series includes MODIS surface reflectance, Enhanced Vegetation Index (EVI), MODIS Bidirectional Reflectance Distribution Function (BRDF), and other ancillary data (Friedl et al., 2002). We used the International Geosphere Biosphere Program (IGBP; (Loveland et al., 2001)) classification data layer provided by the MODIS land cover data set. Albedo values were sampled for all forest types that comprised more than 10% of a given ecoregion's forest area. Thus, for some ecoregions, we have produced multiple reforestation trajectories, each to a different end forest type.

We sampled albedo from the MODIS collection 6 BRDF/Albedo daily 500 m product (MCD43A3) (Schaaf & Wang, 2015). The MODIS albedo product provides both black-sky and white-sky albedo for MODIS bands 1–7 as well as three broad bands spanning the visible, near-infrared, and the shortwave frequencies (Schaaf et al., 2002). Black-sky and white-sky albedos represent the fraction of radiation reflected by the surface under direct illumination as a function of solar zenith angle, or diffuse isotropic illumination, respectively (Schaaf et al., 2002). We sampled shortwave broadband black-sky and white-sky albedo data for all dates available between 2014 and 2018. Within each data tile, we used quality assurance (QA) flags (flagged as “0”) to ensure that only the highest-quality values were included, removing all retrievals involving cloud cover and those flagged for low quality. We stratified the sampling of albedo by snow-free and snow-covered conditions based on the corresponding snow cover condition defined at a pixel level by the MODIS snow cover daily 500-m product (MCD43A2 (Hall & Riggs, 2021; Salomonson & Appel, 2004)). The snow product uses the Normalized Difference Snow Index (NDSI) to identify snow cover conditions. The resulting four component albedo conditions were combined with monthly diffuse fraction and monthly snow cover fraction data to compute monthly blue-sky albedo as described further below (see Equation 1).

2.1.4. Solar Radiation Diffuse and Direct Fractions

To generate blue-sky albedos from diffuse and direct components, we estimated monthly white-sky (diffuse) and black-sky (direct) fractions of incoming shortwave radiation from a climatology of mean monthly National Center for Atmospheric Research (NCAR) National Centers for Environmental Prediction (NCEP) diffuse and direct incoming surface solar radiation reanalysis data provided on a Gaussian grid (T62 with 94 × 192 points) (Kalnay et al., 1996; Kistler et al., 2001) and drawn from a sufficiently representative climatological period computed for 1981 to 2010.

2.1.5. Snow-Covered Fraction

To generate monthly averaged albedos across snow-covered and snow-free conditions, we computed a climatology of monthly snow-covered condition for each pixel from a MODIS snow cover data product, representing the temporal and spatial average occurrence of snow cover in a given month of the year. Present-day snow cover was taken from the MODIS/Terra Snow Cover Monthly L3 Global 0.05Deg CMG, Version 6 (Hall et al., 2002), which provides monthly averages computed from daily snow cover observations in the MODIS/Terra Snow Cover Daily L3 Global 0.05Deg CMG (MOD10C1) data set. We used all available monthly values from March 2000 to August 2021 and averaged them into a monthly "climatology."

2.1.6. Radiative Kernels

Because the study's emphasis is on the climate effect of albedo change, we used radiative kernels to translate a surface-level (i.e., local) albedo change to a top-of-atmosphere radiative forcing that operates at the global climate level. We estimated the radiatively effective annualized blue-sky albedo change in each ecoregion by sampling albedo radiative kernels for all grid cells within each ecoregion, averaging across six different data sources. We converted monthly radiative kernels to a scalar representing each month's fraction of the annual sum, and applied these as scalar weights to the blue-sky albedo for each month. This rescaled monthly changes in albedo to their radiatively effective contribution to an annual climate effect. We used radiative kernels from five different global climate models, namely CAM3, CAM5, ECHAM6, HadGEM2, and HadGEM3, and one radiation budget model, CACKv1.0 (Bright & O'Halloran, 2019; Pendergrass et al., 2018; Shell et al., 2008; Smith, 2018; Smith et al., 2020). Within each ecoregion, we assigned the mean radiative kernel for all pixels in the ecoregion.

2.2. Generating Chronosequences of Blue-Sky Albedo

For each ecoregion, we created a space-for-time substitution chronosequence of monthly blue-sky albedo from the grassland, non-forest condition through to forests of age 1–150 years in 5-year intervals. We use grassland as the initial pre-forest cover type because it is the land cover type that most commonly experiences conversion to forest, and we sample only those ecoregions that naturally support forest cover. While forest stands arrived at their year-2010 age from any non-forest starting condition, whether it be shrubland, grassland, or some other land cover type, we assume a grassland starting condition, but this is only at the 0-year age. Beginning with a grassland initial condition, rather than some other cover type, could influence the magnitude of albedo decline, but it is not expected to alter the timing of the decline to its minimum, only the shape of decline in the first few decades of the chronosequence. Also worth noting is that the shape of albedo dynamics with forest age may vary with local ecological, hydrological, and soil conditions with detail that is not resolved with this study's ecoregional-level sampling.

Monthly albedo samples were drawn from the years 2014 to 2018 with sampling from different stand ages pooled in 5-year bins, then temporally aligned to represent a chronosequence from 0 to 150 years after forest initiation (Figure 1). We shifted the albedo data by 6 years to account for the average temporal lag in the albedo sampling (2014–2018) relative to the forest age map (2010). For the non-forest initial condition, we sampled the albedo of pixels classified as grassland. For years 1–30 along the reforestation trajectory, we sampled albedos for five land cover classes, including grassland, shrubland, savanna, woody savanna, and a given end forest type. The non-forest cover classes were included because reforestation involves a gradual increase in tree cover that does not immediately lead to a pixel being classified as forested and often involves progression through these other land cover classes such as from grassland to a shrub or savanna class and ultimately to the end forest type, typically spanning about 30 years. We tested alternative breakpoints such as 50 and 70 years and found little sensitivity of the results. To continue the chronosequence from 31 to 150 years, only pixels of the end forest type were sampled for a given age bin. We restricted the analysis to 150 years because very few forests are managed to an age beyond 150 years and sampling of such older forests is severely limited. This sampling approach yielded month-specific chronosequences from 0 to 150 years in 5-year bins. In these chronosequences, surface albedo was estimated for each month of the year and in each ecoregion as a function of time since forest initiation, with a unique sampling for each forest type present in the ecoregion. Sampling was performed for two snow-cover conditions (snow-covered and snow-free) crossed by two solar illumination conditions (diffuse and direct illumination) yielding a total sampling population of 74 ecoregions × 12 months × 2 snow conditions × 2 solar illumination conditions × the number of end forest types in each ecoregion. While nearly full coverage of age-class bins is displayed

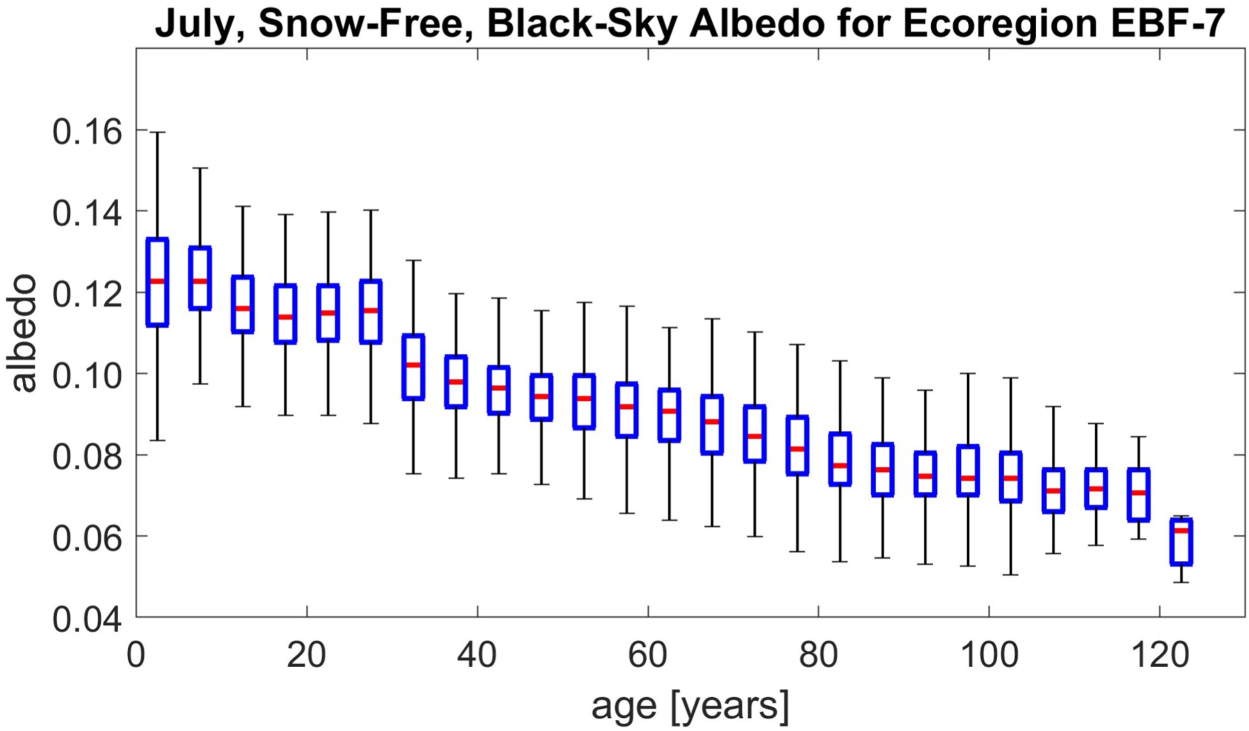

Figure 1. Albedo declines with stand age sampled for each ecoregion. Albedo was sampled in 5-year stand age classes for each individual ecoregion, and for each end forest type existing in that region. Boxplots show frequency distribution statistics (minimum and maximum after removal of outliers, lower and upper quartiles, and median) for July snow-free black-sky albedo sampled from evergreen broadleaf forest locations within an ecoregion in China ("EBF-7"). Full sampling spanned all months of the year for snow-free and snow-covered conditions for both black-sky and white-sky illumination.

in the example in Figure 1, some samplings had gaps in ages and others missed the oldest age classes out to 150 years. Associated data are available (Williams, 2026).

From this sampling, we then generated temporally continuous, annually resolved albedo trajectories from 0 to 150 years using a spline curve-fitting technique. This helped to address gaps and spurious sources of variability present in the sampling across forest age bins. We adopted a Shape Language Modeling (SLM) tool (D'Errico, 2022) to perform a least-squares spline modeling with a flexible range of controls. After careful testing, we set SLM parameters as follows: (a) use intervals or "knots" over which the spline segments were fit, dividing the 0–150 years period into five, 25-year intervals segments, (b) use no shape constraints or slope constraints for spline fits other than to require a linear shape from 0 to 30 years, (c) impose biophysical minimum and maximum albedo limits of 0 and 1 set at both 0 and 150 years, and (d) use a constant value for extrapolation of albedo beyond the oldest 5 years age bin that was populated with sample data. We chose 30 years as the first breakpoint to be consistent with the sampling approach used in generating the chronosequence, whereby the first 30 years included a mix of forest and other woody land cover types. We note that the methods and data sources lend themselves to a more robust characterization of the year-by-year albedo changes from 30- to 150-year stand ages, with a linear response imposed over the first 30 years. Associated code is available (Williams, 2026).

We gap-filled the resulting spline-fit curves to address missing values arising from limited sampling, such as due to lack of snow-cover in certain biomes and months. For example, there were no snow-covered values for ENF and MF from June to September in some of the ecoregions of the middle latitudes. While these values are rarely needed in practical applications (e.g., snow-covered conditions in the tropics), this gap-filling ensures that all theoretically possible conditions have been characterized. For each month that is missing data for a given reforestation trajectory, we filled values with an average of available curves from other ecoregions or months with the following rules: (a) use the same month of the year from the same biome, hemisphere, and continent; (b) use the same month from the same biome and hemisphere but across continents; and (c) use the mean value of the adjacent months from the same biome, hemisphere, and continent. Though rare, if still unfilled, we averaged curves for a given forest type and month drawing from any region globally. Associated code is available (Williams, 2026).

Finally, with the gap-filled, continuously defined data set, we calculated blue-sky monthly albedo from the weighted combination of snow-covered/snow-free and direct/diffuse illumination conditions as follows:

$$\text{BlueSA} = \text{BSA}_{\text{ns}} * \left(1 - f_s\right) * \left(1 - f_r\right) + \text{BSA}_{\text{sc}} * f_s * \left(1 - f_r\right) + \text{WSA}_{\text{ns}} * \left(1 - f_s\right) * f_r + \text{WSA}_{\text{sc}} * f_s * f_r \qquad (1)$$

where f_s is an ecoregion's snow-covered fraction in a given month, f_r is an ecoregion's diffuse light fraction in a given month, subscript ns refers to no-snow and sc refers to snow-covered. We then computed the weighted-average annual blue-sky albedo from radiation-kernel-weighted monthly blue-sky albedos, thus representing the *radiatively effective* average annual albedo change with forest aging. In our analysis, we extracted the median albedo at each age from all curves for all ecoregions within a given combination of forest type and ecoclimatic setting. We sampled the resulting median curves to select the albedo and age (Age80) at which 80% of the total decline from the pre-forest condition is achieved. We focused on 80% of the maximal decline because it is close to the maximal decline while still being approached linearly in time, avoiding the gradual decline to a minimum value that we noticed for that final 20% of decline. Associated computation and analysis code is available (Williams, 2026).

2.3. Statistical Analyses of Ecoclimatic Variation

We stratified the global sample population of Age80 by two strata, ecoclimatic setting and forest type, and examined variation within and between groups of each stratum. We computed associated summary statistics including medians, confidence intervals, 25th and 75th percentiles, and interquartile ranges, and displayed distributions in boxplots. Given the non-Gaussian distribution and unbalanced sampling, we performed an analysis of variance of each stratum using Kruskal-Wallis nonparametric rank-sum tests to evaluate if group medians differ significantly, followed by multiple comparisons tests of pairwise differences between medians. Associated analysis code is available (Williams, 2026).

2.4. Global Mapping of Time to Decline

We generated a global map of Age80 as a summary display of our findings, intended to aid practitioners who may wish to apply these results when accounting for the albedo-induced climate effect of reforestation activities. We assigned the median Age80 for each unique combination of ecoclimate and forest type (see Figure S2 in Supporting Information S1), adopting the most likely end-forest type from Hasler et al. (2024) (see Figure S3 in Supporting Information S1). We also generated a map series sampling the median percentage of decline in 20-year age increments, again using each ecoregion's ecoclimate and most likely end-forest type.

3. Results

Albedo declines from an initial high value in grassland to lower values for forests of all kinds (Figure 2, all relationships significant at $P < 0.0001$). Albedo continues to decline for several decades as forests develop, with a roughly linear approach to a minimum value for most cases (Figure 2). The decline continues to be linear beyond the first 30 years during which the fit was forced to be linear. A rebound in albedo at the oldest ages can be seen in several cases after it reaches a minimum around 80–120 years, but this late-stage increase does not return to the initial non-forested value (e.g., Figure 2).

The timing of albedo's decline differs across ecoclimatic settings (Figure 3, Tables S1–S3 in Supporting Information S1). It is faster in tropical and boreal climates than in temperate climates. Differences across climates are especially pronounced for woody savannas (Figure S2 in Supporting Information S1). The time to reach 80% of the maximum decline in albedo, which we here forth label as "Age80," generally takes 53–63 years in tropical, boreal/taiga, and tundra ecoclimates, 54–85 years in forests of temperate coniferous, temperate grassland/shrubland, temperate broadleaf mixed forest and montane grassland/shrubland ecoclimates, and 100–120 years in temperate Mediterranean ecoclimatic settings (Figure 3, Table S1 in Supporting Information S1: with values referring to 25th and 75th percentiles). Variation in Age80 within individual ecoclimatic types can be large, with interquartile ranges as high as 54% of the median, though tropical climates display relatively tight distributions.

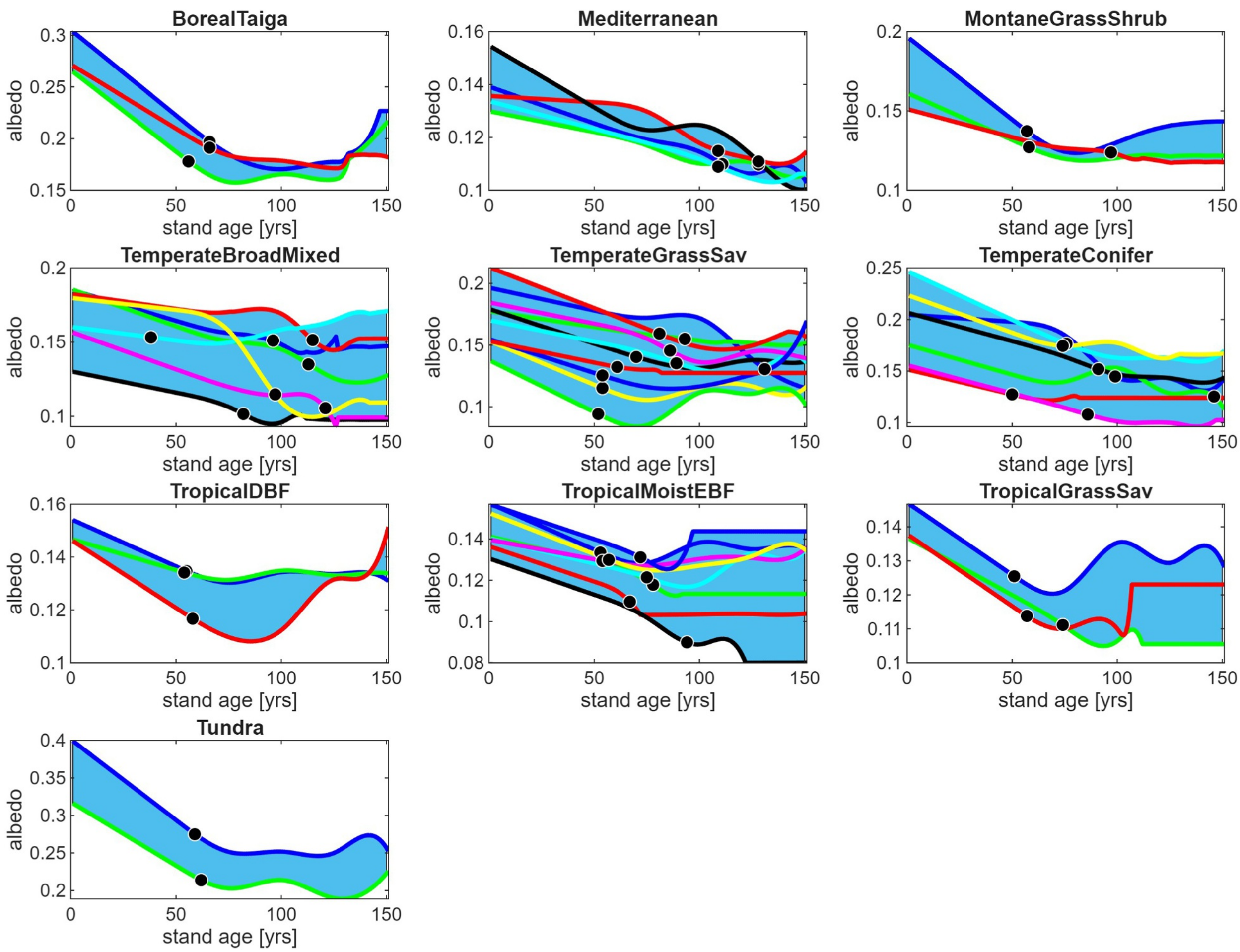

Figure 2. Shape and variability of reforestation-driven albedo decline across ecoclimates and ecoregions. Each plot depicts, for a given ecoclimate, the median radiation kernel-weighted annualized blue-sky albedo as it changes over time with stand age for regrowth of woody savanna. We use woody savanna as an example forest type because it is present in all ecoclimates, but we show results for other forest types in the supplement. Results for individual ecoregions are shown with different line colors in each subplot cycling through nine color options. Cyan shading in the background spans the minimum and maximum of the distribution for a given age across ecoregions. Black dots along the median curve represent the age at which 80% of the maximum decline is first detected. BorealTaiga = boreal forest/taiga; Mediterranean = Mediterranean forests, woodlands and scrub; MontaneGrassShrub = montane grassland and shrublands; TemperateBroadMix = temperate broadleaf and mixed forest; TemperateGrassSav = temperate grasslands, savannas, and shrublands; TemperateConifer = temperate conifer forest; TropicalDBF = tropical deciduous broadleaf forest; TropicalMoistEBF = tropical moist evergreen broadleaf forest; TropicalGrassSav = tropical grasslands and savannas; Tundra = tundra.

The timing of albedo's decline also differs across forest types (Figure 4) but this factor accounts for a smaller proportion of total variability in Age80 than ecoclimatic setting, with only 17% of variance explained by forest types compared to 32% for ecoclimatic setting (Tables S2 and S4 in Supporting Information S1). Median Age80 falls within the range of 56–66 years for most forest types, but for woody savanna it jumps to 74 years (Figure 4, Tables S3 and S4 in Supporting Information S1). Variation in Age80 within individual forest types is small for EBF and DNF (<6%), intermediate for MF and DBF (>23%), and large for ENF and WSA (41% and 54%, respectively). Findings regarding how the timing of albedo declines vary with forest types and ecoclimatic settings were broadly robust to different sampling points along the curves, such as the time to reach 70% or 90% of the maximum decline in albedo (Figures S9 and S10 in Supporting Information S1).

Map display combines these influences of forest type and ecoclimatic conditions to show the geographic patterns emerging from their joint distribution. One map displays the age at which 80% of the maximum decline occurs (Figure 5). A second image displays a map series showing the albedo, expressed as a percentage of the maximum decline, that occurs at different age intervals, from 20 to 100 years in 20-year increments (Figure 6). Northern boreal forests and tropical forests both reach their maximum albedo decline relatively rapidly, whereas temperate forests show a relatively gradual approach. The slowest progression is in areas with a Mediterranean climate,

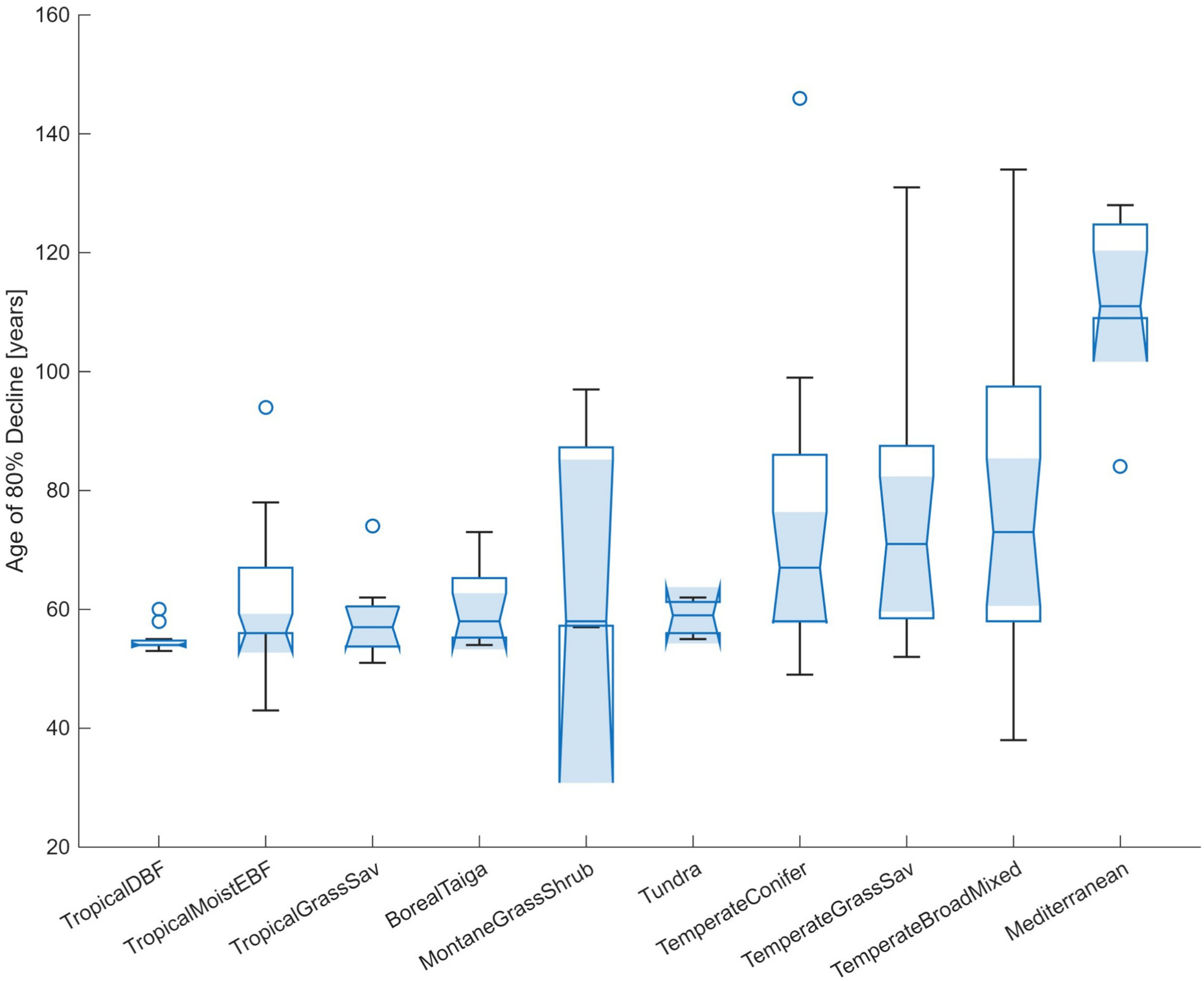

Figure 3. Rate of albedo decline to its minimum varies substantially across ecoclimates. Albedo declines toward its minimum with forest maturation are faster in most tropical settings, more gradual in some temperate, montane, and tundra settings, and particularly slow for the Mediterranean climate. On each box, the central mark indicates the median and the bottom and top edges of the box indicate the 25th and 75th percentiles, respectively. The whiskers extend to the most extreme data points not considered outliers and the outliers are plotted individually with circles. The tapered, blue shaded region of each box indicates its notch, or the 95% confidence interval on the median. Boxes whose notches do not overlap have different medians at a 5% significance level. In some cases, the interquartile range (lower 25th or 75th percentile of the data) extends less far than the notch.

likely linked to moisture limitation that leads to slow growth of low-stature trees. By 80 years, most locations have reached 90% or more of the maximum decline. These maps are intended to serve as tools for practitioners needing to quantify the near-term climate benefits that may be achieved from reforestation within the next several decades. For example, someone seeking to adjust carbon credits to account for an albedo driven warming could first determine the magnitude of change from Hasler et al. (2024) and then determine the fraction of that change to apply using the 20 years increments (Figure 6).

4. Discussion and Conclusions

This study documents the decline in surface albedo with reforestation over time in different ecoclimatic settings around the world. Similar to the gradual accumulation of biomass that ensues with forest maturation and development, we see a gradual approach to a minimum albedo that unfolds over decades. Its magnitude and timing vary across forest types and ecoclimatic settings, taking about 40–70 years to realize half of the warming effect from albedo change, and anywhere from 50 to 120 years to reach 80% of the full decline in albedo. The fastest declines are found in fast-growing tropical, humid environments, and in forests with needleleaf trees. The

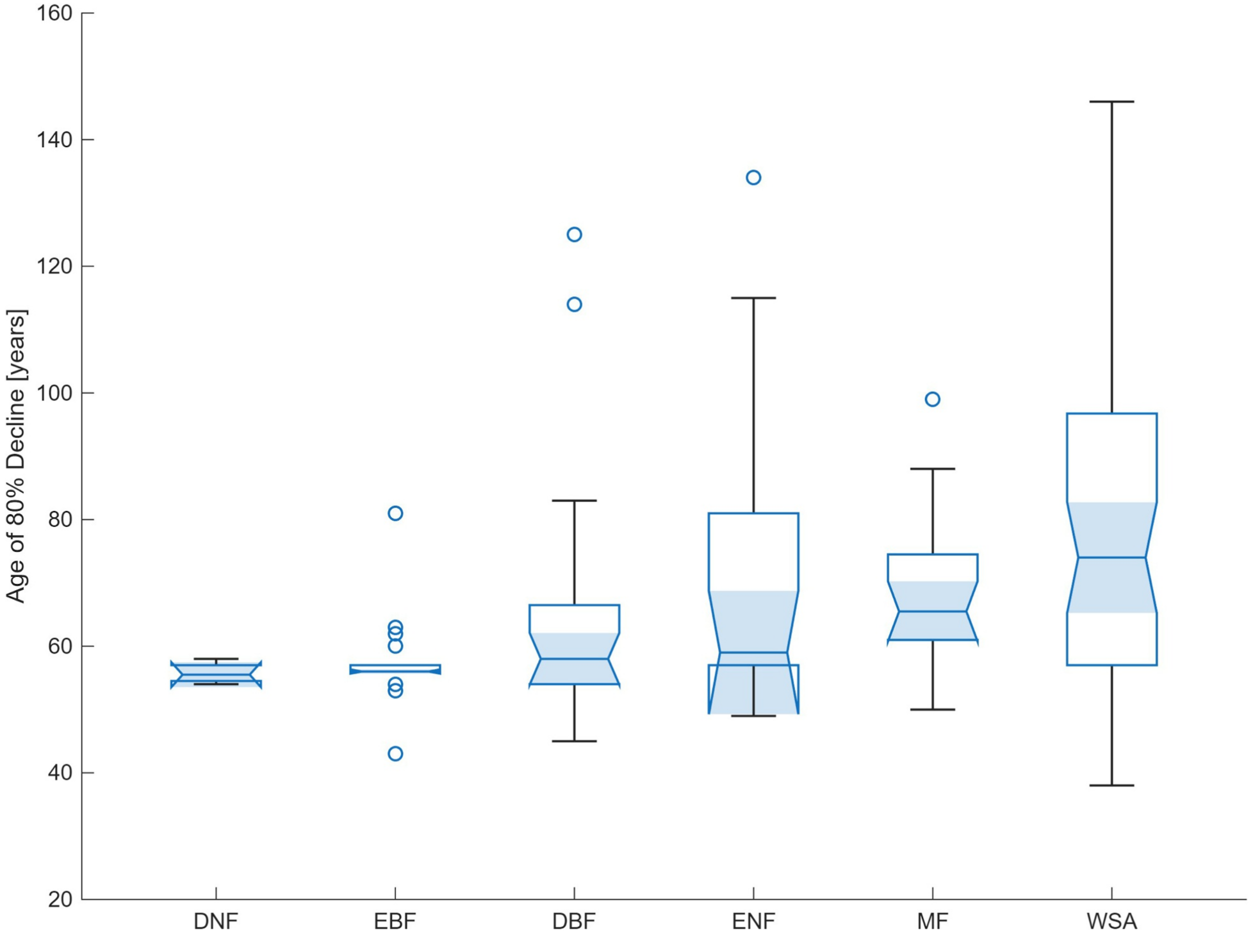

Figure 4. Rate of albedo decline to its minimum varies little across forest types. The rate of albedo declines toward its minimum with forest maturation is generally similar across forest types except for woody savannahs, which take longer to reach their minimum albedo with stand age. EBF = evergreen broadleaf forest, DNF = deciduous needleleaf forest, ENF = evergreen needleleaf forest, DBF = deciduous broadleaf forest, MF = mixed forest, WSA = woody savanna. On each box, the central mark indicates the median and the bottom and top edges of the box indicate the 25th and 75th percentiles, respectively. The whiskers extend to the most extreme data points not considered outliers and the outliers are plotted individually with circles. The tapered, blue shaded region of each box indicates its notch, or the 95% confidence interval on the median. Boxes whose notches do not overlap have different medians at a 5% significance level. In some cases, the interquartile range (lower 25th or 75th percentile of the data) extends less far than the notch.

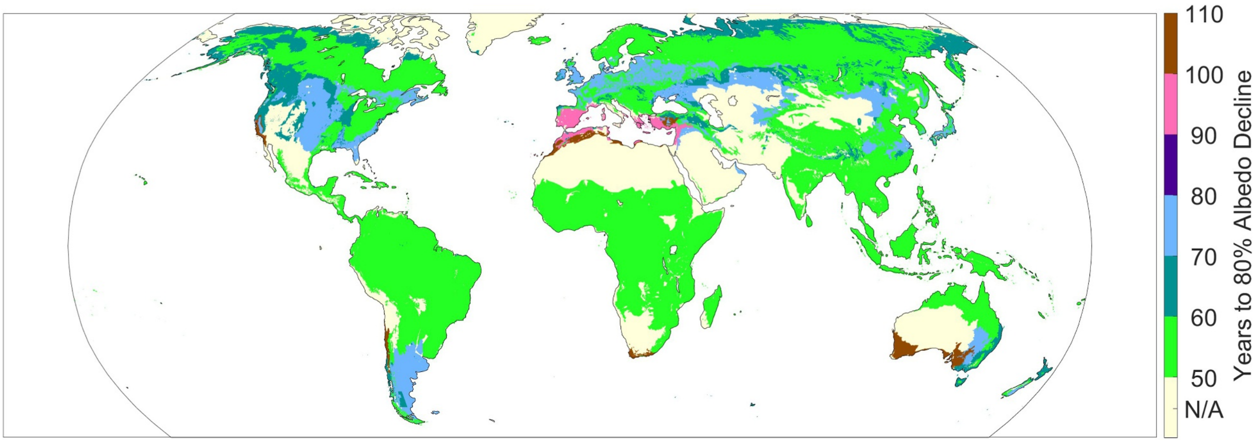

Figure 5. Global variation in the time (years) it takes to reach 80% of the maximum albedo decline. The decline in albedo with forest development is relatively fast in most tropical settings, more gradual in some temperate, montane, and tundra settings, and particularly slow in Mediterranean climate settings.

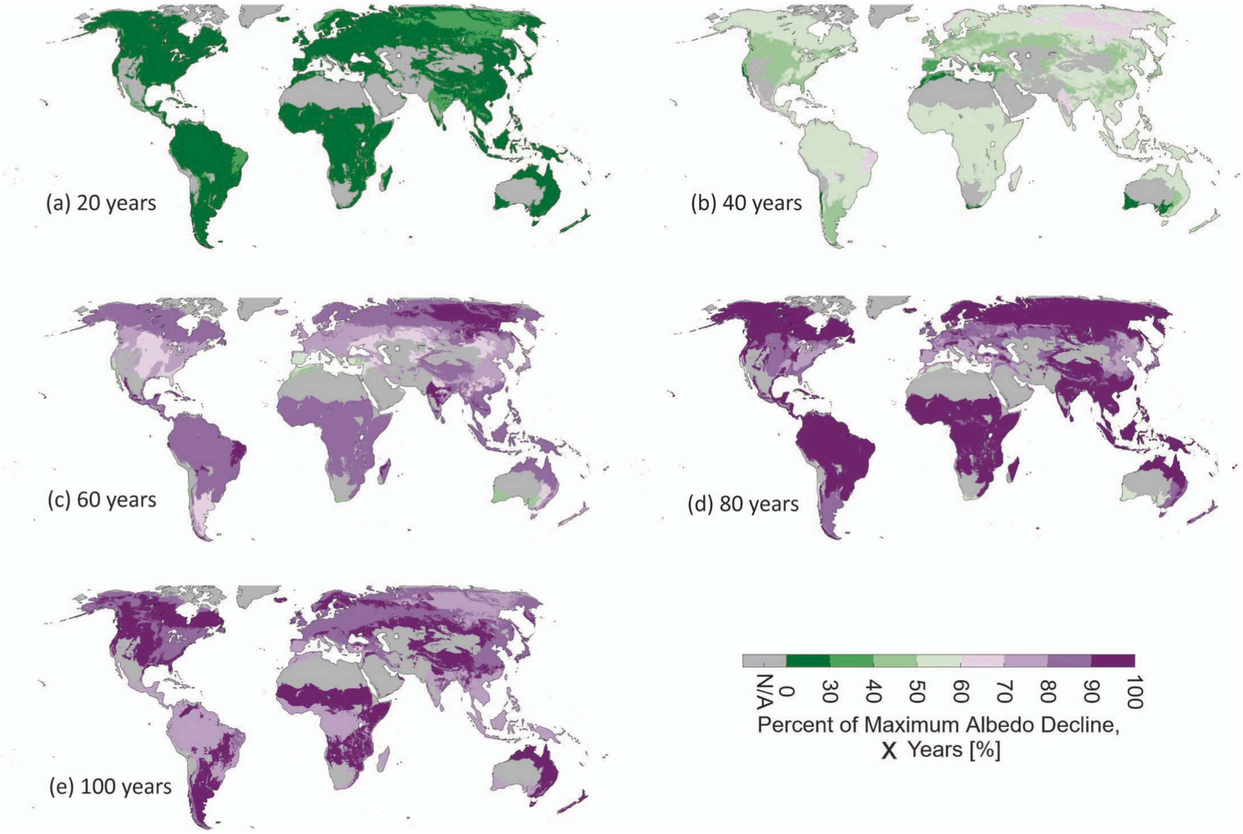

Figure 6. Global variation in the percentage of maximum albedo decline by a stand age of X years. X varies across subpanels as (a) 20 years, (b) 40 years, (c) 60 years, (d) 80 years, and (e) 100 years.

largest declines appear in extra-tropical environments and in needleleaf or mixed forest types, including cold temperate and boreal regions with substantial wintertime snow cover.

Ecoclimate and forest type conditions explain only part of the variation in Age80, with wide spread in distributions for some combinations, for example, woody savanna in temperate coniferous ecoclimate (Figure S2 in Supporting Information S1). The distribution of Age80 tends to be asymmetric, with a positive skew toward high values, indicating that the median value for a given forest type may not be representative in all cases. After several decades of decline to a minimum albedo, some locations exhibited a rebound toward higher values (Figure 6). We surmise that this rebound could be related to mortality-driven canopy openings that uncover a brighter understory, or conversely to canopy closure that decreases within-canopy shadowing and shading, as reported by Yan et al. (2021).

The timing of albedo declines with forest age is in broad alignment with the range reported in prior studies from various regions around the world. Several early studies of Scandinavian boreal forests indicated relatively rapid declines to a minimum. For example, a study of spruce, pine, and birch forests in Norway and Sweden (Bright et al., 2013) showed that, in warmer months (10°C), MODIS albedo declined to 69%, 64%, and 51% of the initial value within 100 years, and reached 80% of the maximum decline within 20–25 years. In colder months (0°C), declines were larger (58%, 51%, and 34%) and the decline to a minimum value took longer (20, 25, and 100 years). Regarding magnitude, albedo declined from around 0.45 to 0.23 in the colder season and 0.35 to 0.13 in the warmer season. Another study of the same forest types and region (Kuusinen et al., 2014) indicated similar findings, with shortwave albedo declines to a minimum generally taking 30 years, a somewhat slower decline in spruce compared to pine stands, and larger albedo declines in winter than summer. In summer, albedo declined from approximately 0.13 to 0.08 for young to mature forests, and in winter from 0.58 to 026. Although direct comparisons are not easily achieved because of different sampling strategies, these magnitudes overlap with this study's declines for ENF, DNF, DBF, and WSA forests in boreal and temperate ecoregions. Another point of comparison can be drawn from studies of albedo in North American forests after a harvest or fire disturbance. One such study, from mixed boreal forests of Ontario, Canada reported albedo declines exhibiting a negative exponential shape reaching 80% of the maximum decline in about 30 years post-harvest and slightly longer post-fire (by 40 years) (Halim et al., 2019). Winter albedos declined from around 0.72 to 0.20 in winter and 0.23 to 0.08 in summer. In a US-wide study, Healey et al. (2025) sampled Landsat albedos of different forest types and stand ages in a chronosequence and computed radiative forcing of change relative to local non-forest to generate a time-dependent emissions-equivalent CO_2 flux. Analysis of their results indicates an average Age80 of 118 ± 36 years (1 standard deviation) across all forest types, with 25th, 50th, and 75th percentiles of 100, 110, and 130 years. Finally, a broad synthesis of in situ measurements from global FLUXNET and AmeriFlux stations, though largely concentrated in North America and Europe, indicated a general decline in albedo reaching 80% of the maximum decline by 60 years in evergreen forests but not until 120 years for deciduous forests (Zhu et al., 2024). Albedo declines were larger in evergreen stands, falling from 0.29 to 0.10 in the first 100 years on average, whereas deciduous stands saw declines from 0.19 to 0.15. Taken together, the shape, timing, and magnitude of albedo declines with forest aging vary widely across unique geographic settings, and this study's new global analysis is broadly consistent with tendencies reported in prior studies for specific regions and forest types.

This study's direct use of the MODIS daily albedo product helps capture local details over global geographies. However, sampling with the relatively low spatial resolution of the MODIS albedo data product (500 m × 500 m) presents some challenges. The primary concern is sub-pixel variation in MODIS land cover type, whereby there is a dominant land cover type that is assigned at the MODIS 500 m × 500 m data product scale but that may encompass other land cover types within the moderate resolution pixel. This can be an issue where land cover types change over short distances, leading to mixed pixels in the sampling. For example, the global albedo atlas of Gao et al. (2014) involved careful sampling of "pure" pixels for which the surface cover is almost entirely composed of the intended biome type. This study's use of the MODIS albedo data set was not able to perform the same screening to isolate pure pixels; thus, it included mixed pixels that will be composed of both target and non-target surface cover classes. This would tend to reduce the difference in the albedo change that we detected in this study. Although the albedo atlas produced by Gao et al. (2014) has some advantages of identifying pixels with a more homogeneous and singular vegetated condition and land cover type, it was not suitable for this study because its finest resolution (0.05°) is incompatible for integration with finer resolution forest stand age data, which varies over tens to hundreds of meters. The mixed pixel effect in the present study could be expected to exact a consistent error in the estimation of median albedo for different age classes, such that the temporal pattern is still robust to this issue. Thus, despite this sampling limitation, we still expect this study's approach to have produced a reliable characterization of the timing of albedo declines with forest development, which was the main purpose of the study. Other studies provide better estimates of the magnitude of change (e.g., Hasler et al., 2024).

There is also a risk that forest age may have been reset during the time intervening between the forest age data set (2010) and the albedo data sampling (2014–2018). We consulted the Global Forest Watch data set to get a sense of the rate of ecoregional age-resetting disturbance rates and found that they tend to be less than 1% per year but can be as high as about 2.5% per year in rare cases. A rate of 1% per year over 6 years would affect about 6% of our samples, while 2.5% per year would reach 15% of samples. We expect this to factor into sampling noise such that it does not significantly bias the results, especially given our use of median as the key statistic. It is also worth noting that patches of severe disturbance are often smaller than the scale of the 500 m × 500 m MODIS albedo pixels. Such large pixels can be expected to contain a range of forest ages, and likely include some effects of recent disturbances. Future work, as described below, should consider ways to filter out all MODIS-albedo-scale pixels that had more than a modest amount of the area experience a stand-resetting disturbance during the temporal window between the stand age data and albedo-sampling.

Future work may be able to resolve the aforementioned challenges by leveraging higher spatial resolution reflectance data such as from Landsat or Sentinel-2 albedo data products (Franch et al., 2014, 2018, 2019; He et al., 2018; Lin et al., 2022; Shuai et al., 2011). However, those higher resolution albedo data products have been produced only for limited places and times and are not operationally available with widespread coverage at this time. Higher resolution sampling may also enable more detailed exploration of how forest composition, canopy structural properties, soil properties, topography and other factors that influence the magnitude and timing of albedo declines with forest maturation. Employing machine learning techniques to extract emergent patterns is also likely to be a fruitful pursuit. Hopefully, these and other advancements will explain additional variation and provide a more detailed depiction of albedo dynamics with temporal and spatial variability in forests.

Reforestation continues to draw attention as a leading natural climate solution (Bastin et al., 2019; Cook-Patton et al., 2020; Drever et al., 2021; Griscom et al., 2017; Law et al., 2018; Pan et al., 2011; Walker et al., 2022). Here we show that, when assessing the climate forcing of reforestation, it is important to take account of the gradual effects of both biomass and albedo changes that unfold as tree cover increases and forests mature. Just as it takes a century or more for biomass carbon to be sequestered in forest carbon stocks, the albedo effect unfolds gradually over several decades as well. A comprehensive, time-bound accounting framework, such as that discussed by Bright and Lund (2021), is necessary to fully characterize these biogeochemical and biogeophysical effects on the climate system that ensue with reforestation. Currently, few forest carbon standards include albedo corrections, as albedo accounting is still nascent (Riley et al., 2025). So far, only one standard (Isometric) directly incorporates albedo into its methodology, though albedo is more commonly used to evaluate and rate projects during due diligence processes. However, we know of none that account for their effect over time.

The map displaying the time for albedo to decline with reforestation (Figure 6) is designed for use by practitioners who need to include albedo considerations in the management and policy of forest-based natural climate solutions. In using this map to inform carbon standard methodology development and land stewardship decision-making, we recommend deriving a more robust estimate of the magnitude of albedo change from Hasler et al. (2024) and then use the data in Figure 6 to determine what fraction of that change has occurred at the relevant 20-year interval. Assuming a linear change between time points is a simplifying assumption that is broadly consistent with this study's findings and would support direct application. As such, the temporal dynamics of albedo change with stand age could be readily taken into consideration by mitigation planners and land managers who seek to quantify the net climate opportunity from reforestation in different areas of the globe.

Conflict of Interest

The authors declare no conflicts of interest relevant to this study.

Availability Statement

Primary sample data and codes for computing secondary data and for analysis supporting the results in the paper have been published and are available as a published data set (Williams, 2026). This includes the median black/white sky and snow-covered/snow-free albedos for each stand age class and for each ecoregion and each end forest type that was used in the study to generate the curve-fit chronosequences. Codes for curve fitting, gap-filling, and data analysis are provided. Metadata reporting the relevant climatological attributes of each ecoregion are also provided.

Acknowledgments
This work was funded by a Bezos Earth Fund grant to The Nature Conservancy with an associated sub-award to Clark University.

References

Amiro, B. D., Orchansky, A. L., Barr, A. G., Black, T. A., Chambers, S. D., Chapin, F. S., et al. (2006). The effect of post-fire stand age on the boreal forest energy balance. *Agricultural and Forest Meteorology*, *140*(1–4), 41–50. https://doi.org/10.1016/j.agrformet.2006.02.014

Bastin, J.-F., Finegold, Y., Garcia, C., Mollicone, D., Rezende, M., Routh, D., et al. (2019). The global tree restoration potential. *Science*, *365*(6448), 76–79. https://doi.org/10.1126/science.aax0848

Bathiany, S., Claussen, M., Brovkin, V., Raddatz, T., & Gayler, V. (2010). Combined biogeophysical and biogeochemical effects of large-scale forest cover changes in the MPI Earth system model. *Biogeosciences*, *7*(5), 1383–1399. https://doi.org/10.5194/bg-7-1383-2010

Beck, H. E., Zimmermann, N. E., McVicar, T. R., Vergopolan, N., Berg, A., & Wood, E. F. (2018). Present and future Köppen-Geiger climate classification maps at 1-km resolution. *Scientific Data*, *5*(1), 180214. https://doi.org/10.1038/sdata.2018.214

Besnard, S., Koirala, S., Santoro, M., Weber, U., Nelson, J., Gütter, J., et al. (2021). Mapping global forest age from forest inventories, biomass and climate data. *Earth System Science Data*, *13*(10), 4881–4896. https://doi.org/10.5194/essd-13-4881-2021

Betts, R. A. (2000). Offset of the potential carbon sink from boreal forestation by decreases in surface albedo. *Nature*, *408*(6809), 187–190. https://doi.org/10.1038/35041545

Betts, R. A., Falloon, P. D., Goldewijk, K. K., & Ramankutty, N. (2007). Biogeophysical effects of land use on climate: Model simulations of radiative forcing and large-scale temperature change. *Agricultural and Forest Meteorology*, *142*(2), 216–233. https://doi.org/10.1016/j.agrformet.2006.08.021

Bonan, G. B. (2008). Forests and climate change: Forcings, feedbacks, and the climate benefits of forests. *Science*, *320*(5882), 1444–1449. https://doi.org/10.1126/science.1155121

Bright, R. M., Astrup, R., & Strømman, A. H. (2013). Empirical models of monthly and annual albedo in managed boreal forests of interior Norway. *Climatic Change*, *120*(1), 183–196. https://doi.org/10.1007/s10584-013-0789-1

Bright, R. M., Eisner, S., Lund, M. T., Majasalmi, T., Myhre, G., & Astrup, R. (2018). Inferring surface albedo prediction error linked to forest structure at high latitudes. *Journal of Geophysical Research: Atmospheres*, *123*(10), 4910–4925. https://doi.org/10.1029/2018JD028293

Bright, R. M., & Lund, M. T. (2021). CO_2-equivalence metrics for surface albedo change based on the radiative forcing concept: A critical review. *Atmospheric Chemistry and Physics*, *21*(12), 9887–9907. https://doi.org/10.5194/acp-21-9887-2021

Bright, R. M., & O'Halloran, T. L. (2019). Developing a monthly radiative kernel for surface albedo change from satellite climatologies of Earth's shortwave radiation budget: CACK v1.0. *Geoscientific Model Development*, *12*(9), 3975–3990. https://doi.org/10.5194/gmd-12-3975-2019

Bright, R. M., Zhao, K., Jackson, R. B., & Cherubini, F. (2015). Quantifying surface albedo and other direct biogeophysical climate forcings of forestry activities. *Global Change Biology*, *21*(9), 3246–3266. https://doi.org/10.1111/gcb.12951

Busch, J., Bukoski, J. J., Cook-Patton, S. C., Griscom, B., Kaczan, D., Potts, M. D., et al. (2024). Cost-effectiveness of natural forest regeneration and plantations for climate mitigation. *Nature Climate Change*, *14*(9), 996–1002. https://doi.org/10.1038/s41558-024-02068-1

Cook-Patton, S. C., Leavitt, S. M., Gibbs, D., Harris, N. L., Lister, K., Anderson-Teixeira, K. J., et al. (2020). Mapping carbon accumulation potential from global natural forest regrowth. *Nature*, *585*(7826), 545–550. https://doi.org/10.1038/s41586-020-2686-x

Davin, E. L., & de Noblet-Ducoudre, N. (2010). Climatic impact of global-scale deforestation: Radiative versus nonradiative processes. *Journal of Climate*, *23*(1), 97–112. https://doi.org/10.1175/2009jcli3102.1

D'Errico, J. (2022). SLM—Shape language modeling. (Version). Retrieved from https://www.mathworks.com/matlabcentral/fileexchange/24443-slm-shape-language-modeling

Dinerstein, E., Olson, D., Joshi, A., Vynne, C., Burgess, N. D., Wikramanayake, E., et al. (2017). An ecoregion-based approach to protecting half the terrestrial realm. *BioScience*, *67*(6), 534–545. https://doi.org/10.1093/biosci/bix014

Drever, C. R., Cook-Patton, S. C., Akhter, F., Badiou, P. H., Chmura, G. L., Davidson, S. J., et al. (2021). Natural climate solutions for Canada. *Science Advances*, *7*(23), eabd6034. https://doi.org/10.1126/sciadv.abd6034

Foley, J. A., DeFries, R., Asner, G. P., Barford, C., Bonan, G., Carpenter, S. R., et al. (2005). Global consequences of land use. *Science*, *309*(5734), 570–574. https://doi.org/10.1126/science.1111772

Franch, B., Vermote, E., Skakun, S., Roger, J.-C., Santamaria-Artigas, A., Villaescusa-Nadal, J. L., & Masek, J. (2018). Toward Landsat and Sentinel-2 BRDF normalization and albedo estimation: A case study in the Peruvian Amazon Forest. *Frontiers in Earth Science*, *6*(185), 185. https://doi.org/10.3389/feart.2018.00185

Franch, B., Vermote, E., Skakun, S., Roger, J.-C., Masek, J., Ju, J., et al. (2019). A method for Landsat and Sentinel 2 (HLS) BRDF normalization. *Remote Sensing*, *11*(6), 632. https://doi.org/10.3390/rs11060632

Franch, B., Vermote, E. F., & Claverie, M. (2014). Intercomparison of Landsat albedo retrieval techniques and evaluation against in situ measurements across the US SURFRAD network. *Remote Sensing of Environment*, *152*, 627–637. https://doi.org/10.1016/j.rse.2014.07.019

Friedl, M. A., McIver, D. K., Hodges, J. C. F., Zhang, X. Y., Muchoney, D., Strahler, A. H., et al. (2002). Global land cover mapping from MODIS: Algorithms and early results. *Remote Sensing of Environment*, *83*(1), 287–302. https://doi.org/10.1016/S0034-4257(02)00078-0

Gao, F., He, T., Wang, Z., Ghimire, B., Shuai, Y., Masek, J. G., et al. (2014). Multiscale climatological albedo look-up maps derived from moderate resolution imaging spectroradiometer BRDF/albedo products. *Journal of Applied Remote Sensing*, *8*(1), 083532. https://doi.org/10.1117/1.JRS.8.083532

Ghimire, B., Williams, C. A., Masek, J., Gao, F., Wang, Z., Schaaf, C., & He, T. (2014). Global albedo change and radiative cooling from anthropogenic land cover change, 1700 to 2005 based on MODIS, land use harmonization, radiative kernels, and reanalysis. *Geophysical Research Letters*, *41*(24), 9087–9096. https://doi.org/10.1002/2014gl061671

Griscom, B. W., Adams, J., Ellis, P. W., Houghton, R. A., Lomax, G., Miteva, D. A., et al. (2017). Natural climate solutions. *Proceedings of the National Academy of Sciences*, *114*(44), 11645–11650. https://doi.org/10.1073/pnas.1710465114

Halim, M. A., Chen, H. Y. H., & Thomas, S. C. (2019). Stand age and species composition effects on surface albedo in a mixedwood boreal forest. *Biogeosciences*, *16*(22), 4357–4375. https://doi.org/10.5194/bg-16-4357-2019

Hall, D., & Riggs, G. (2021). *MODIS/Terra snow cover daily L3 global 0.05Deg CMG, version 61*. NASA National Snow and Ice Data Center Distributed Active Archive Center. https://doi.org/10.5067/MODIS/MOD10C1.061

Hall, D. K., Riggs, G. A., Salomonson, V. V., DiGirolamo, N. E., & Bayr, K. J. (2002). MODIS snow-cover products. *Remote Sensing of Environment*, *83*(1), 181–194. https://doi.org/10.1016/S0034-4257(02)00095-0

Hasler, N., Williams, C. A., Denney, V. C., Ellis, P. W., Shrestha, S., Terasaki Hart, D. E., et al. (2024). Accounting for albedo change to identify climate-positive tree cover restoration. *Nature Communications*, *15*(1), 2275. https://doi.org/10.1038/s41467-024-46577-1

He, T., Liang, S., Wang, D., Cao, Y., Gao, F., Yu, Y., & Feng, M. (2018). Evaluating land surface albedo estimation from Landsat MSS, TM, ETM+, and OLI data based on the unified direct estimation approach. *Remote Sensing of Environment*, *204*, 181–196. https://doi.org/10.1016/j.rse.2017.10.031

Healey, S. P., Yang, Z., Erb, A. M., Bright, R. M., Domke, G. M., Frescino, T. S., & Schaaf, C. B. (2025). Enhanced observation of forest albedo reveals significant offsets to reported carbon benefits. *Environmental Research Letters*, *20*(7), 074025. https://doi.org/10.1088/1748-9326/add60a

Jackson, R. B., Randerson, J. T., Canadell, J. G., Anderson, R. G., Avissar, R., Baldocchi, D. D., et al. (2008). Protecting climate with forests. *Environmental Research Letters*, *3*(4), 044006. https://doi.org/10.1088/1748-9326/3/4/044006

Jiao, T., Williams, C. A., Ghimire, B., Masek, J., Gao, F., & Schaaf, C. (2017). Global climate forcing from albedo change caused by large-scale deforestation and reforestation: Quantification and attribution of geographic variation. *Climatic Change*, *142*(3), 463–476. https://doi.org/10.1007/s10584-017-1962-8

Juang, J.-Y., Katul, G., Siqueira, M., Stoy, P., & Novick, K. (2007). Separating the effects of albedo from eco-physiological changes on surface temperature along a successional chronosequence in the southeastern United States. *Geophysical Research Letters*, *34*(21). https://doi.org/10.1029/2007GL031296

Kalnay, E., Kanamitsu, M., Kistler, R., Collins, W., Deaven, D., Gandin, L., et al. (1996). The NCEP/NCAR 40-year reanalysis project. *Bulletin of the American Meteorological Society*, *77*(3), 437–471. https://doi.org/10.1175/1520-0477(1996)077<0437:tnyrp>2.0.co;2

Kirschbaum, M. U. F., Whitehead, D., Dean, S. M., Beets, P. N., Shepherd, J. D., & Ausseil, A. G. E. (2011). Implications of albedo changes following afforestation on the benefits of forests as carbon sinks. *Biogeosciences*, *8*(12), 3687–3696. https://doi.org/10.5194/bg-8-3687-2011

Kistler, R., Kalnay, E., Collins, W., Saha, S., White, G., Woollen, J., et al. (2001). The NCEP–NCAR 50-year reanalysis: Monthly means CD-ROM and documentation. *Bulletin of the American Meteorological Society*, *82*(2), 247–268. https://doi.org/10.1175/1520-0477(2001)082<0247:tnnyrm>2.3.co;2

Kuusinen, N., Tomppo, E., Shuai, Y., & Berninger, F. (2014). Effects of forest age on albedo in boreal forests estimated from MODIS and Landsat albedo retrievals. *Remote Sensing of Environment*, *145*, 145–153. https://doi.org/10.1016/j.rse.2014.02.005

Law, B. E., Hudiburg, T. W., Berner, L. T., Kent, J. J., Buotte, P. C., & Harmon, M. E. (2018). Land use strategies to mitigate climate change in carbon dense temperate forests. *Proceedings of the National Academy of Sciences*, *115*(14), 3663–3668. https://doi.org/10.1073/pnas.1720064115

Lawrence, D., Coe, M., Walker, W., Verchot, L., & Vandecar, K. (2022). The Unseen Effects of Deforestation: Biophysical Effects on Climate. *Frontiers in Forests and Global Change*, *5*, 756115. https://doi.org/10.3389/ffgc.2022.756115

Lin, X., Wu, S., Chen, B., Lin, Z., Yan, Z., Chen, X., et al. (2022). Estimating 10-m land surface albedo from Sentinel-2 satellite observations using a direct estimation approach with Google Earth Engine. *ISPRS Journal of Photogrammetry and Remote Sensing*, *194*, 1–20. https://doi.org/10.1016/j.isprsjprs.2022.09.016

Loveland, T., Reed, B., Brown, J., Ohlen, D., Zhu, J., Yang, L., & Merchant, J. (2001). Development of a global land cover characteristics database and IGBP DISCover from 1-km AVHRR data. *International Journal of Remote Sensing*, *20*(6–7), 1303–1330. https://doi.org/10.1080/014311600210191

O'Halloran, T. L., Law, B. E., Goulden, M. L., Wang, Z., Barr, J. G., Schaaf, C., et al. (2012). Radiative forcing of natural forest disturbances. *Global Change Biology*, *18*(2), 555–565. https://doi.org/10.1111/j.1365-2486.2011.02577.x

Pan, Y., Birdsey, R. A., Fang, J., Houghton, R., Kauppi, P. E., Kurz, W. A., et al. (2011). A large and persistent carbon sink in the world's forests. *Science*, *333*(6045), 988–993. https://doi.org/10.1126/science.1201609

Pendergrass, A. G., Conley, A., & Vitt, F. M. (2018). Surface and top-of-atmosphere radiative feedback kernels for CESM-CAM5. *Earth System Science Data*, *10*(1), 317–324. https://doi.org/10.5194/essd-10-317-2018

Pongratz, J., Reick, C. H., Raddatz, T., & Claussen, M. (2010). Biogeophysical versus biogeochemical climate response to historical anthropogenic land cover change. *Geophysical Research Letters*, *37*(8). https://doi.org/10.1029/2010gl043010

Riley, L. M., Cook-Patton, S. C., Albert, L. P., Still, C. J., Williams, C. A., & Bukoski, J. J. (2025). Accounting for albedo in carbon market protocols. *Nature Communications*, *16*(1), 8810. https://doi.org/10.1038/s41467-025-64317-x

Rohatyn, S., Yakir, D., Rotenberg, E., & Carmel, Y. (2022). Limited climate change mitigation potential through forestation of the vast dryland regions. *Science*, *377*(6613), 1436–1439. https://doi.org/10.1126/science.abm9684

Rotenberg, E., & Yakir, D. (2010). Contribution of semi-arid forests to the climate system. *Science*, *327*(5964), 451–454. https://doi.org/10.1126/science.1179998

Salomonson, V. V., & Appel, I. (2004). Estimating fractional snow cover from MODIS using the normalized difference snow index. *Remote Sensing of Environment*, *89*(3), 351–360. https://doi.org/10.1016/j.rse.2003.10.016

Schaaf, C., & Wang, Z. (2015). MCD43A3 MODIS/Terra+Aqua BRDF/Albedo Daily L3 Global—500m V006 [Dataset]. https://doi.org/10.5067/MODIS/MCD43A3.006

Schaaf, C. B., Gao, F., Strahler, A. H., Lucht, W., Li, X. W., Tsang, T., et al. (2002). First operational BRDF, albedo nadir reflectance products from MODIS. *Remote Sensing of Environment*, *83*(1–2), 135–148. https://doi.org/10.1016/S0034-4257(02)00091-3

Shell, K. M., Kiehl, J. T., & Shields, C. A. (2008). Using the radiative kernel technique to calculate climate feedbacks in NCAR's community atmospheric model. *Journal of Climate*, *21*(10), 2269–2282. https://doi.org/10.1175/2007jcli2044.1

Shrestha, S., Williams, C. A., Rogers, B. M., Rogan, J., & Kulakowski, D. (2022). Wildfire controls on land surface properties in mixed conifer and ponderosa pine forests of Sierra Nevada and Klamath Mountains, Western US. *Agricultural and Forest Meteorology*, *320*, 108939. https://doi.org/10.1016/j.agrformet.2022.108939

Shrestha, S., Williams, C. A., Rogers, B. M., Rogan, J., & Kulakowski, D. (2024). Divergent biophysical responses of western United States forests to wildfire driven by eco-climatic gradients. *Biogeosciences*, *21*(9), 2207–2226. https://doi.org/10.5194/bg-21-2207-2024

Shuai, Y., Masek, J. G., Gao, F., & Schaaf, C. B. (2011). An algorithm for the retrieval of 30-m snow-free albedo from Landsat surface reflectance and MODIS BRDF. *Remote Sensing of Environment*, *115*(9), 2204–2216. https://doi.org/10.1016/j.rse.2011.04.019

Smith, C. J. (2018). HadGEM2 radiative kernels [Dataset]. *University of Leeds*. https://doi.org/10.5518/406

Smith, C. J., Kramer, R. J., Myhre, G., Alterskjær, K., Collins, W., Sima, A., et al. (2020). Effective radiative forcing and adjustments in CMIP6 models. *Atmospheric Chemistry and Physics*, *20*(16), 9591–9618. https://doi.org/10.5194/acp-20-9591-2020

Vanderhoof, M., Williams, C. A., Ghimire, B., & Rogan, J. (2013). Impact of mountain pine beetle outbreaks on forest albedo and radiative forcing, as derived from Moderate Resolution Imaging Spectroradiometer, Rocky Mountains, USA. *Journal of Geophysical Research: Biogeosciences*, *118*(4), 1461–1471. https://doi.org/10.1002/jgrg.20120

Vanderhoof, M., Williams, C. A., Shuai, Y., Jarvis, D., Kulakowski, D., & Masek, J. (2014). Albedo-induced radiative forcing from mountain pine beetle outbreaks in forests, south-central Rocky Mountains: Magnitude, persistence, and relation to outbreak severity. *Biogeosciences*, *11*(3), 563–575. https://doi.org/10.5194/bg-11-563-2014

Veldman, J. W., Overbeck, G. E., Negreiros, D., Mahy, G., Le Stradic, S., Fernandes, G. W., et al. (2015). Where tree planting and forest expansion are bad for biodiversity and ecosystem services. *BioScience*, *65*(10), 1011–1018. https://doi.org/10.1093/biosci/biv118

Walker, W. S., Gorelik, S. R., Cook-Patton, S. C., Baccini, A., Farina, M. K., Solvik, K. K., et al. (2022). The global potential for increased storage of carbon on land. *Proceedings of the National Academy of Sciences*, *119*(23), e2111312119. https://doi.org/10.1073/pnas.2111312119

Weber, J., King, J. A., Abraham, N. L., Grosvenor, D. P., Smith, C. J., Shin, Y. M., et al. (2024). Chemistry-albedo feedbacks offset up to a third of forestation's CO_2 removal benefits. *Science*, *383*(6685), 860–864. https://doi.org/10.1126/science.adg6196

Williams, C. A. (2026). Global variation in the timing of albedo declines with reforestation and forest aging Version 2 [Dataset]. https://doi.org/10.5281/zenodo.20128644

Williams, C. A., Gu, H., & Jiao, T. (2021). Climate impacts of U.S. forest loss span net warming to net cooling. *Science Advances*, *7*(7), eaax8859. https://doi.org/10.1126/sciadv.aax8859

Yan, H., Wang, S., Dai, J., Wang, J., Chen, J., & Shugart, H. H. (2021). Forest greening increases land surface albedo during the main growing period between 2002 and 2019 in China. *Journal of Geophysical Research: Atmospheres*, *126*(6), e2020JD033582. https://doi.org/10.1029/2020JD033582

Zhang, Q., Barnes, M., Benson, M., Burakowski, E., Oishi, A. C., Ouimette, A., et al. (2020). Reforestation and surface cooling in temperate zones: Mechanisms and implications. *Global Change Biology*, *26*(6), 3384–3401. https://doi.org/10.1111/gcb.15069

Zhu, Q., Chen, J., Charles, P.-A. B., Sonnentag, O., Montagnani, L., O'Halloran, T. L., et al. (2024). Albedo-induced global warming potential following disturbances in global temperate and boreal forests. *Journal of Geophysical Research: Biogeosciences*, *129*(3), e2023JG007848. https://doi.org/10.1029/2023JG007848